Web-based Supporting Materials for "Dynamic Predictions in Bayesian Functional Joint Models for Longitudinal and Time-to-Event Data: An Application to Alzheimer's Disease"

1 Hippocampus Image Processing

For image processing, we adopt a surface fluid registration package[1] which has been used in various studies[2–5]. The original imaging data, 3D brain MRI scans, are downloaded from `www.loni.ucla.edu/ADNI`. The first step is the extraction of the left and right hippocampi surfaces from original MRI scans using FIRST[6], an integrated surface analysis tool developed as part of the FSL library[7]. The surface is the outer layer of the brain region and has an inherent 2D structure. Then the surface is modeled as a mesh of triangles for each side of the hippocampi. Each triangle is know as a face. The place where the corners of the triangles meet is called a vertex. The coordinates (i.e., the X, Y, and Z) at each vertex are determined from the MRI during the extraction process. Before conducting the registration, each surface are first conformally mapped to a 2D rectangle plane using holomorphic 1-forms. This process is similar to unfolding a paper bag. A feature image of the surface is computed from this conformal representation and registered to a chosen template image via inverse consistent surface fluid registration. Using conformal mapping, the surface registration problem is essentially converted into an image registration problem. The registered feature image can be recovered into the original hippocampal surface based on coordinates. Detailed image processing and registration procedure can be found in Shi *et al*[1].

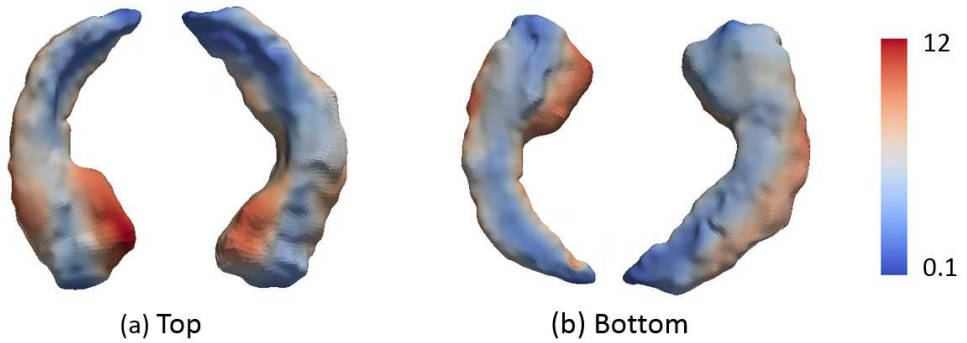

Figure 1: The top and bottom views of one MCI patient's hippocampal radial distance denoted by colors.

Each registered feature image corresponding to the either left or right hippocampal surfaces contains 15,000 vertices. Knowledge of the coordinates of the vertices allows us to compute several surface statistics, including radial distance, multivariate tensor-based morphometry (mTBM), determinant of the Jacobian matrix, and two eigenvalues of the Jacobian matrix. Specifically, we adopt radial distance as our target measurement. Figure 1 displays the hippocampus surface morphology of one patient with radial distance being coded in colors. In the final step, the points on the feature image, which have one-to-one correspondence of the vertices on the surface, are vectorized. In this way, the corresponding radial distances of the points are aligned to form a one-dimensional functional predictor denoted by $g_i^{(x)}(s)$. Because the study of population variation in the registered image is of interest, the spatial variation is not intentionally modeled in our analysis. The coefficient function $B^{(x)}(s)$ is defined on the same domain as $g_i^{(x)}(s)$ and it can be easily mapped to the surface domain. Figure 2 displays the data processing procedure along with an illustration of a functional joint model.

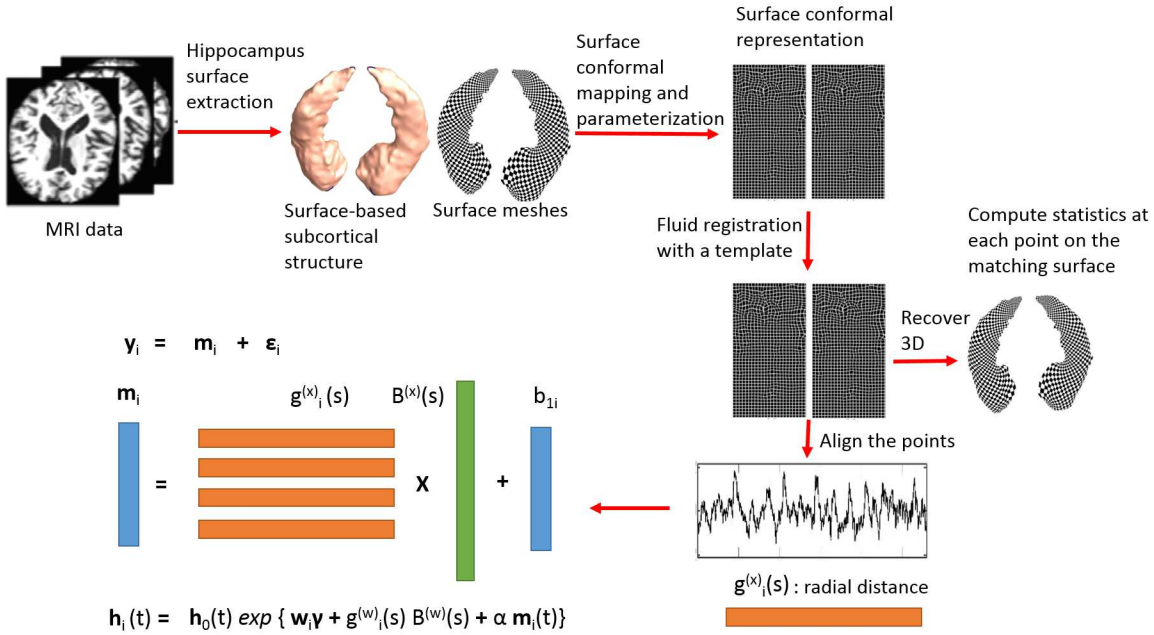

Figure 2: Hippocampus image processing procedure along with an illustration of a functional joint model.

2 Application to the ADNI Study

Table 1: The estimated coefficients for the 20 FPC scores derived from hippocampal radial distance (HRD) in longitudinal submodel (3) of model $FJM3$.

Parameters	Mean	SE	2.5%	97.5%
$B_1^{(x)}$	1.063	0.593	−0.087	2.185
$B_2^{(x)}$	0.893	0.884	−0.892	2.619
$B_3^{(x)}$	−0.694	0.981	−2.595	1.210
$B_4^{(x)}$	1.701	1.347	−0.922	4.284
$B_5^{(x)}$	2.586	1.463	−0.312	5.466
$B_6^{(x)}$	−3.368	1.568	−6.434	−0.335
$B_7^{(x)}$	−2.101	1.674	−5.376	1.242
$B_8^{(x)}$	1.117	1.845	−2.399	4.741
$B_9^{(x)}$	1.594	1.983	−2.205	5.507
$B_{10}^{(x)}$	−4.391	2.096	−8.511	−0.033
$B_{11}^{(x)}$	0.646	2.372	−4.132	5.279
$B_{12}^{(x)}$	1.345	2.329	−3.129	5.799
$B_{13}^{(x)}$	2.944	2.403	−2.012	7.661
$B_{14}^{(x)}$	−0.891	2.470	−5.889	3.801
$B_{15}^{(x)}$	−3.929	2.594	−9.197	1.185
$B_{16}^{(x)}$	−5.610	2.986	−11.260	0.228
$B_{17}^{(x)}$	0.702	2.830	−4.851	6.134
$B_{18}^{(x)}$	6.988	2.968	1.101	12.840
$B_{19}^{(x)}$	0.121	3.098	−5.727	6.132
$B_{20}^{(x)}$	0.715	3.159	−5.199	6.954

Table 2: The estimated coefficients for the 20 FPC scores derived from hippocampal radial distance (HRD) in survival submodel (4) of model $FJM3$.

Parameters	Mean	SE	2.5%	97.5%
$B_1^{(w)}$	0.875	0.132	0.647	1.123
$B_2^{(w)}$	−0.073	0.213	−0.510	0.273
$B_3^{(w)}$	0.091	0.203	−0.336	0.471
$B_4^{(w)}$	0.360	0.250	−0.162	0.801
$B_5^{(w)}$	0.010	0.318	−0.538	0.678
$B_6^{(w)}$	0.790	0.363	0.240	1.601
$B_7^{(w)}$	−1.161	0.328	−1.795	−0.455
$B_8^{(w)}$	1.001	0.367	0.384	1.754
$B_9^{(w)}$	−0.702	0.377	−1.422	0.088
$B_{10}^{(w)}$	−0.320	0.652	−1.245	1.019
$B_{11}^{(w)}$	−3.635	0.456	−4.426	−2.644
$B_{12}^{(w)}$	−0.184	0.507	−0.920	0.817
$B_{13}^{(w)}$	0.954	0.835	−0.247	2.755
$B_{14}^{(w)}$	−3.051	0.888	−4.788	−1.350
$B_{15}^{(w)}$	0.720	0.396	−0.058	1.424
$B_{16}^{(w)}$	−1.745	0.862	−3.246	0.041
$B_{17}^{(w)}$	1.818	0.771	0.532	3.273
$B_{18}^{(w)}$	−1.255	1.125	−3.152	1.048
$B_{19}^{(w)}$	0.288	0.892	−1.720	1.817
$B_{20}^{(w)}$	−0.028	0.964	−1.635	2.017

3 Stan code for the simulation study

```
 data {
  int<lower=0> I; // Number of subjects in training data
  int<lower=0> obs_long; // Number of observations
  int subj_long[obs_long];  // Subject index for each observation
  real Y[obs_long];
  real X[obs_long];
  real W[I];
  int Kx;  // Number of FPC score
  int Kb;  // Number of knots for B-spline
  vector[Kx] AX[I]; // FPC score for functional predictor gX
  vector[Kx] AW[I]; // FPC score for functional predictor gW
  real<lower=0> time[I];  // Survival time
  int<lower=0> event[I];  // Censoring indicator
  matrix[Kx, Kb] M_matX;  // \int phi(s)psi(s) ds
  matrix[Kx, Kb] M_matW;  //
}

parameters {
  vector[2] beta;
  vector[Kb] BX;
  real b[I];
  real gamma;
  vector[Kb] BW;
  real alpha;
  real logscale;
  real tau_b;
  real tau_Y;
  real sigma_BX;
  real sigma_BW;
}

transformed parameters {
  real sigma_b;
  real sigma_Y;
  real sigma2_b;
  real sigma2_Y;
  real tau_BX;
  real tau_BW;
```

```
  vector[Kb] MxGamX;
  vector[Kb] MxGamW;

  vector[I] etaX; // estimated \int gX(s)BX(s) ds
  vector[I] etaW; // estimated \int gW(s)BW(s) ds
  real mu[obs_long];

  sigma_b <- pow(tau_b, -0.5);
  sigma_Y <- pow(tau_Y, -0.5);
  sigma2_b <- pow(tau_b, -1);
  sigma2_Y <- pow(tau_Y, -1);
  tau_BX <- pow(sigma_BX, -1);
  tau_BW <- pow(sigma_BW, -1);

  // construct the functional components in the model
  MxGamX <- M_matX *BX ;
  MxGamW <- M_matW *BW ;

  for(i in 1:I){
    etaX[i] <- MxGamX' * AX[i];
    etaW[i] <- MxGamW' * AW[i];
  }

  // construct the unobserved true trajectory
  for (ob in 1:obs_long){
    mu[ob] <- beta[1] + X[ob]*beta[2] + etaX[subj_long[ob]] + b[subj_long[ob]];
  }
}

model {
  real h[I];
  real S[I];
  real LL[I];

  // construct random effect
  b ~ normal(0, sigma_b);
  // construct the longitudinal submodel
  Y ~ normal(mu, sigma_Y);
```

```
  // construct the survival submodel
  for(i in 1:I){
    h[i] <- exp(logscale+gamma*W[i] + etaW[i] + alpha*(beta[1] +
            beta[2]*time[i] + etaX[i] +b[i]));
    S[i] <- exp(-exp(logscale+gamma*W[i] + etaW[i] + alpha*(beta[1] + etaX[i] + b[i]))*
            (exp(alpha*beta[2]*time[i])-1)/(alpha*beta[2]));
    LL[i] <- log(pow(h[i],event[i])*S[i]);
  }

  increment_log_prob(LL);


  // construct the priors
  beta ~ normal(0,10);
  gamma ~ normal(0,10);

  BX[1] ~ normal(0, sigma_BX);
  BW[1] ~ normal(0, sigma_BW);
  for(p in 2:Kb){
    BX[p] ~ normal(BX[p-1], sigma_BX);
    BW[p] ~ normal(BW[p-1], sigma_BW);
  }

  alpha ~ normal(0,10);
  logscale ~ normal(0, 10);
  tau_Y ~ gamma(0.01,0.01);
  tau_b ~ gamma(0.01,0.01);

  sigma_BX ~ inv_gamma(0.01,0.01);
  sigma_BW ~ inv_gamma(0.01,0.01);

}
```

References

[1] Shi J, Thompson PM, Gutman B, Wang Y, Initiative ADN, et al. Surface fluid registration of conformal representation: Application to detect disease burden and genetic influence on hippocampus. NeuroImage. 2013;78:111–134.

[2] Colom R, Stein JL, Rajagopalan P, Martínez K, Hermel D, Wang Y, et al. Hippocampal structure and human cognition: Key role of spatial processing and evidence supporting the efficiency hypothesis in females. Intelligence. 2013;41(2):129–140.

[3] Luders E, Thompson PM, Kurth F, Hong JY, Phillips OR, Wang Y, et al. Global and regional alterations of hippocampal anatomy in long-term meditation practitioners. Human Brain Mapping. 2013;34(12):3369–3375.

[4] Monje M, Thomason ME, Rigolo L, Wang Y, Waber DP, Sallan SE, et al. Functional and structural differences in the hippocampus associated with memory deficits in adult survivors of acute lymphoblastic leukemia. Pediatric Blood & Cancer. 2013;60(2):293–300.

[5] Shi J, Wang Y, Ceschin R, An X, Lao Y, Vanderbilt D, et al. A multivariate surface-based analysis of the putamen in premature newborns: regional differences within the ventral striatum. PLOS ONE. 2013;8(7):e66736.

[6] Patenaude B, Smith SM, Kennedy DN, Jenkinson M. A Bayesian model of shape and appearance for subcortical brain segmentation. NeuroImage. 2011;56(3):907–922.

[7] Jenkinson M, Beckmann CF, Behrens TE, Woolrich MW, Smith SM. FSL. NeuroImage. 2012;62(2):782–790.